Acta of Bioengineering and Biomechanics
Vol. 26, No. 2, 2024

Original paper
DOI: 10.37190/ABB-02415-2024-03

The biomechanical implications of lacunar and perilacunar microarchitecture on microdamage accumulation in cortical bone

XIUYAN YANG[1], XICHEN CHEN[1], CHUNHUI JI[1]*, LIANG ZHANG[1], CHUANBIN YAN[1], BIN LIN[1], JUAN DU[2], ZHEN WANG[3]

[1] School of Mechanical Engineering, Tianjin University, Tianjin, China.
[2] Academy of Medical Engineering and Translational Medicine, Tianjin University, Tianjin, China.
[3] School of Mechanical Engineering, Yanshan University, Hebei, China.

Purpose: This study aimed to explore how the microarchitectural features of lacunae and perilacunar zones impact the biomechanics of microdamage accumulation in cortical bone, crucial for understanding bone disorders' pathogenesis and developing preventive measures. *Methods*: Utilizing the phase field finite element method, the study analyzed three bone unit models with varying microarchitecture: one without lacunae, one with lacunae and one including perilacunar zones, to assess their effects on cortical bone's biomechanical properties. *Results*: The presence of lacunae was found to increase microcrack initiation risk, acting as nucleation points and accelerating microcrack propagation. Proximity to Haversian canals exacerbated stress concentration, speeding microdamage progression. Conversely, perilacunar zones mitigated both initiation and propagation. An elevated critical energy release rate correlated with slower crack growth and reduced damage severity. *Conclusions*: The research sheds light on the intricate mechanisms governing microcrack behavior in compact bone, highlighting the significant role of bone's microarchitectural features in its biomechanical response to microdamage. These insights are valuable for the development of strategies to prevent and treat bone-related disorders.

Key words: *microdamage accumulation, cortical bone, lacunae, perilacunar zones, phase field method*

1. Introduction

The structural integrity of cortical bone is a complex interplay between its intricate microarchitecture and the physiological processes that maintain its functionality. Microdamage accumulation within the bone matrix is a key determinant of skeletal health and longevity, with microcracks serving as early indicators of potential structural failure [8], [21]. These minuscule defects can trigger a sequence of events that lead to bone remodeling, a critical process for preserving bone strength and resilience [29], [36]. The balance between microdamage formation and repair is delicate as any disruption can lead to increased bone fragility and a higher risk of fractures [6], [13].

The microarchitecture of compact bone with its lacuna-canalicular network, extracellular matrix and endocortical region is vital for generating micro-strains that can lead to microcrack formation [25], [34]. Osteocytes, situated within the mineralized matrix and interconnected by lacunae and canaliculi, are central to the lacuna-canalicular network (LCN). This network is essential for the bone's mechanosensory functions, enabling it to respond to mechanical stimuli [28], [37]. Despite advancements in imaging techniques [14], [26], the exact role of lacunae in microdamage is still debated. Some research indicate that lacunae may intensify stress–strain responses [18], while other studies find a lower incidence of microcracks in areas with high lacunar density [17], [33]. The lacunar voids, more exactly their distribution only influenced the paths of the

* Corresponding author: Chunhui Ji, School of Mechanical Engineering, Tianjin University, Tianjin, China, e-mail: jichunhui@tju.edu.cn
Received: March 11th, 2024
Accepted for publication: June 26th, 2024

microcracks as they propagated through osteocyte lacunae, but neither their size, nor their number [31].

Further investigation using atomic force microscopy to study lacunae formation in young and aged female mice has shown that the modulus difference in the perilacunar zone, influenced by bone cell remodeling, can significantly affect bone tissue quality [35]. This finding underscores the importance of the perilacunar zone's modulus gradation, which is dependent on the recency of osteocyte bone formation [27]. Finite element models have been employed to quantify how changes in lacunar morphology and perilacunar tissue properties affect the local mechanical environment and the mechanosensitivity of bone cells [30]. Collectively, these studies enhance our understanding of the relationship between bone microarchitecture and its mechanical properties, which is crucial for developing strategies to improve bone health and prevent fractures.

The phase field method, a sophisticated computational technique, has been instrumental in advancing our understanding of bone microstructure. It has been used to enhance the fracture resistance of biomimetic designs [7] and to analyze the effects of advanced glycation end products (AGEs) on cortical bone fracture in a two-dimensional model [24]. Additionally, the dynamics of porous bone fractures have been explored using a phase field model, providing insights into the complex processes of crack evolution [4]. These studies complement earlier work that used finite element methods to investigate the relationship between tissue elasticity, lacunar strains and fluid flow around bone cells [10], [18]. However, earlier studies primarily focused on linear elastic tissue behavior, which may not fully capture the complexity of bone's mechanical responses under various conditions.

Recent research has provided new insights into the biomechanics of bone microarchitecture, particularly in relation to the constitutive model for bone and the role of vascularized bone tissues. Establishing a constitutive model for trabecular bone at the microscale to describe the purely elastic response of bone tissue and employing finite element methods to establish the relationship between microstructure and biomechanics [16]. Additionally, a discrete phase model of blood flow in roughened microchannels has been introduced to better understand the biomechanical factors contributing to microdamage in vascularized bone tissues [19]. These studies, in conjunction with the phase field method and finite element models, are essential for a detailed understanding of how bone's microarchitecture influences its biomechanical properties, informing the development of therapeutic strategies for bone-related disorders.

This study aimed to bridge the gap in our understanding of the biomechanical roles of lacunae and perilacunar zones within cortical bone microarchitecture. By employing a comprehensive computational analysis using the phase field finite element method, we aimed to reconcile conflicting views on the impact of these microstructural elements on microcrack behavior. Through the simulation of various microarchitectural configurations, we seeked to elucidate the complex interactions between lacunae, perilacunar zones and bone's mechanical response to stress. This investigation not only refined our knowledge of bone's intrinsic biomechanics but also informed the development of targeted therapeutic strategies and biomimetic materials designed to enhance bone durability and resilience. Ultimately, this research may contribute to the broader objective of preventing bone-related disorders and improving clinical outcomes for patients afflicted with conditions such as osteoporosis and other skeletal fragility syndromes.

2. Materials and methods

2.1. Theory

In the phase field model, the dispersion of cracks can be described by constructing a crack density function [3], [39]. Taking a one-dimensional infinitely long rod as an example, assuming there is a through-crack at $x = 0$, the crack can be represented by a strongly discontinuous scalar field function $D(x)$.

$$D(x) = \begin{cases} 1, & x = 0 \\ 0, & x \neq 0 \end{cases}. \tag{1}$$

Although the strongly discontinuous function accurately describes the location of the crack, it presents challenges in simulating crack propagation. The fracture phase field model employs a continuous field function to simulate the formation of cracks in a diffuse manner, which is more suitable for handling the non-discrete evolution of cracks. An exponential function is introduced to approximate the crack topology, accommodating the continuity of the crack.

$$d(x) = e^{-|x|/l_c}. \tag{2}$$

The length scale parameter, denoted as l_c, governs the regularized or diffuse crack topology represented by the phase field function $d(x)$. The function values $d(0) = 1$ and $d(\infty) = 0$ correspond to the material states

of perfect integrity and complete failure, respectively, while $d(x) \in (0, 1)$ indicates varying degrees of material damage. An increase in l_c results in a larger diffusion region of the phase field, whereas a decrease in l_c confines the diffusion region [38].

Clearly, the phase field distribution function, given by Eq. (2), is the solution to the following homogeneous differential equation:

$$d(x) - l_c^2 d''(x) = 0, \tag{3}$$

with the boundary conditions:

$$d(0) = 1, d(\pm\infty) = 0. \tag{4}$$

Equation (3) is also the Euler equation derived from the variational principle below:

$$d = Arg\{\inf_{d \in W} I(d)\}, \tag{5}$$

where

$$I(d) = \frac{1}{2}\int_{\Omega} (d^2 + l_c^2 d'^2) dV, \tag{6}$$

$$W = \{d \mid d(0) = 0, d(\pm\infty) = 0\}. \tag{7}$$

By substituting $d(x)$ into the functional $I(d)$ and integrating, we obtain:

$$I(d = e^{-|x|/l_c}) = l_c \Gamma. \tag{8}$$

Consequently, the result of the functional integral is related to the crack length parameter l_c and the crack surface Γ. Therefore, a crack surface functional can be defined based on the form of $I(d)$:

$$\Gamma(d) = \frac{1}{l_c} I(d) = \frac{1}{2l_c}\int_{\Omega} (d^2 + l_c^2 d'^2) dV = \int_{\Omega} \gamma(d, d') dV, \tag{9}$$

$$\gamma(d, d') = \frac{1}{2l_c}(d^2 + l_c^2 d'^2). \tag{10}$$

Here, $\gamma(d, d')$ is the one-dimensional crack surface density function. Referring to the definition of the one-dimensional crack surface density function, for two-dimensional and three-dimensional problems, the crack surface density function can be set as:

$$\gamma(d, \nabla d) = \frac{1}{2l_c} d^2 + \frac{l_c}{2} |\nabla d|^2, \tag{11}$$

where ∇d represents the phase field gradient field.

Substituting the discrete forms of displacement field and phase field into the variational form of the traditional phase field model, within quadrilateral isoperimetric elements, we obtain:

$$\delta W(\boldsymbol{u}, \boldsymbol{d}) = (\delta \boldsymbol{u})^T (-\boldsymbol{R}^u) + (\delta \boldsymbol{d})^T (-\boldsymbol{R}^d) = 0, \tag{12}$$

where

$$\boldsymbol{R}^u = -\left[\int_{\Omega^e} w(d)(AD)^T C(AD) \det \boldsymbol{J} d\xi d\eta\right] \boldsymbol{U} + \int_{\Omega^e} \boldsymbol{N}^T \cdot \boldsymbol{f} \det \boldsymbol{J} d\xi d\eta + \int_{\partial\Omega_t} \boldsymbol{N}^T \cdot \boldsymbol{t} dS, \tag{13}$$

$$\boldsymbol{R}^d = -\left\{\int_{\Omega^e} \frac{G_c}{l_0}[\boldsymbol{N}_d^T \boldsymbol{N}_d + l_0^2 (B_d)] \det \boldsymbol{J} d\xi d\eta\right\} d^e - \int_{\Omega^e} w'(d) \psi^+(\varepsilon) \boldsymbol{N}^T \det \boldsymbol{J} d\xi d\eta. \tag{14}$$

Here, C represents the matrix of elastic coefficients.

$$B_d = J^{-1} Q^d d^e, \tag{15}$$

$$Q^d = \begin{bmatrix} \frac{\partial S_i}{\partial \xi} & \frac{\partial S_j}{\partial \xi} & \frac{\partial S_m}{\partial \xi} & \frac{\partial S_n}{\partial \xi} \\ \frac{\partial S_i}{\partial \eta} & \frac{\partial S_j}{\partial \eta} & \frac{\partial S_m}{\partial \eta} & \frac{\partial S_n}{\partial \eta} \end{bmatrix}, \tag{16}$$

$$\boldsymbol{N}_d = [S_i \;\; S_j \;\; S_m \;\; S_n]. \tag{17}$$

Following the conventional finite element method, by assembling the element stiffness matrices and considering the boundary conditions, the solution to the following system of equations is obtained:

$$R^u = 0, \quad R^d = 0. \tag{18}$$

Due to the coupling between the phase field and displacement field, the resulting system of equations is nonlinear, necessitating the use of iterative methods for solving the nonlinear system [23]. Furthermore, the aforementioned equation also serves as the global residual equation in the nonlinear iterative solution process.

The Newton–Raphson (N–R) iterative method is employed to solve the nonlinear system of equations. Assuming that the results obtained at the k-th time step during the l-th iteration are u_l^k and d_l^k, the format for the $(l + 1)$-th iteration is as follows:

$$\begin{Bmatrix} u_{l+1}^k \\ d_{l+1}^k \end{Bmatrix} = \begin{Bmatrix} u_l^k \\ d_l^k \end{Bmatrix} + \begin{bmatrix} \boldsymbol{K}_l^{uu} & \boldsymbol{K}_l^{ud} \\ \boldsymbol{K}_l^{du} & \boldsymbol{K}_l^{dd} \end{bmatrix}^{-1} \begin{Bmatrix} R_l^u \\ R_l^d \end{Bmatrix}, \tag{19}$$

where $\boldsymbol{K}_l^{uu}$, $\boldsymbol{K}_l^{ud}$, $\boldsymbol{K}_l^{du}$, $\boldsymbol{K}_l^{dd}$ is the global tangent stiffness matrix, defined as the partial derivatives of the global residual with respect to u_l^k and d_l^k. These can

be obtained by assembling the element tangent stiffness matrices as follows:

$$\boldsymbol{K}^{uu} = -\frac{\partial R_l^u}{\partial u} = \int_{\Omega^e} w(d)(AD)^T C(AD) \det \boldsymbol{J} d\xi d\eta \,, \tag{20}$$

$$\boldsymbol{K}^{dd} = -\frac{\partial R_l^u}{\partial d^e} = \int_{\Omega^e} w'(d)(AD)^T C(AD) U N_d \det \boldsymbol{J} d\xi d\eta \,, \tag{21}$$

$$\boldsymbol{K}^{du} = -\frac{\partial R_l^u}{\partial U} = \int_{\Omega^e} w'(d)(N_d)^T U^T (AD) C(AD) \det \boldsymbol{J} d\xi d\eta, \tag{22}$$

$$\boldsymbol{K}^{dd} = -\frac{\partial R_l^d}{\partial d^e} = \int_{\Omega^e} H(\psi^+) w''(d)(N_d)^T N_d \det \boldsymbol{J} d\xi d\eta + \int_{\Omega^e} \frac{G_c}{l_0}[(N_d)^T N_d + l_0^2 (B_d)^T (B_d)] \det \boldsymbol{J} d\xi d\eta. \tag{23}$$

To enhance the convergence properties of global iterative schemes, an alternating iteration strategy has been introduced. This strategy operates under the premise that by maintaining one field at a constant value while solving for the other, computational efficiency and convergence can be improved. The convexity of the total energy, which is typically non-convex, is temporarily achieved by holding one field constant, thus simplifying the convergence of the iterative process [2], [12]. The basic steps of the alternating iteration are as follows: given the displacement field u_l and phase field d_l at the l-th iteration, fix the phase field and solve for the displacement field at the $(l + 1)$-th step.

$$u_{l+1} = u_l + [K^{uu}(u_l, d_l)]^{-1} R^u(u_l, d_l) \,. \tag{24}$$

Subsequently, with the displacement field u_{l+1} held constant, the phase field for the $(l + 2)$-th step is calculated as follows:

$$d_{l+2} = d_{l+1} + [K^{dd}(u_{l+1}, d_{l+1})]^{-1} R^d(u_{l+1}, d_{l+1}) \,. \tag{25}$$

Furthermore, Molnar et al. [22] have made additional modifications to the aforementioned algorithm to facilitate its implementation using ABAQUS's user-defined subroutines, with the format being:

$$\begin{Bmatrix} u_{l+1} \\ d_{l+1} \end{Bmatrix} = \begin{Bmatrix} u_l \\ d_l \end{Bmatrix} + \begin{bmatrix} K_l^{uu} & 0 \\ 0 & K_l^{dd} \end{bmatrix}^{-1} \begin{Bmatrix} R_l^u \\ R_l^d \end{Bmatrix}. \tag{26}$$

This enables high computational efficiency using ABAQUS's powerful solver. Unlike the global iterative format, the alternating iteration format omits non-diagonal blocks from the global tangent stiffness matrix, but still accounts for the coupling between the phase and displacement fields.

To implement a fracture phase field model in ABAQUS, a layered approach was employed, incorporating two distinct types of elements. Each layer's elements are connected at the same nodes, providing stiffness contributions with varying degrees of freedom, as illustrated in Fig. 1. The first element type possesses only one degree of freedom, corresponding to the phase field. The second element type contributes two or three degrees of freedom (translation) based on the dimensionality (2D or 3D). In all cases, isoperimetric elements with four nodes (2D) were utilized.

Subsequently, for visualization purposes within ABAQUS, a third layer with infinitesimally small stiffness was introduced, crafted using a User-defined Material Mechanical Behavior (UMAT) subroutine. The primary function of this layer is to facilitate information transfer through shared variables and perform interpolation between integration points.

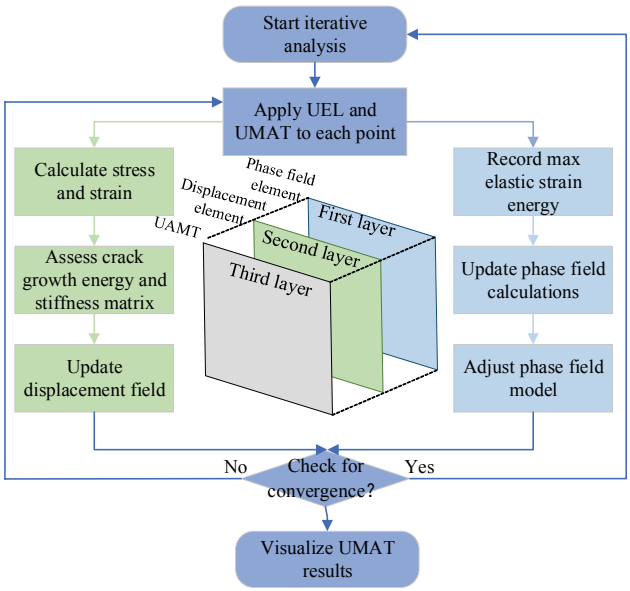

Fig. 1. Flowchart of fracture phase field method based on ABAQUS subroutine

In ABAQUS, a user-defined element subroutine (UEL) is created for a 2D rectangular phase field element with four nodes. Each node has three degrees of freedom, two for displacements and one for the phase field.

The primary procedural steps are as follows:

(1) Determine element type;
(2) Define shape functions;
(3) Establish Gaussian integration points and weights for numerical integration;
(4) Compute shape function values and derivatives at Gaussian points;

(5) Calculate the Jacobian matrix and determinant for coordinate transformation;
(6) Derive the strain matrix B using the strain–displacement relationship;
(7) Compute the element stiffness matrix;
(8) Evaluate Right-Hand Side (RHS) terms';
(9) Update state variables at nodes during the solution process.

The stiffness matrix for displacements is denoted as follows:

$$K^{uu} = -\frac{\partial R_l^u}{\partial u} = \int_{\Omega^e} w(d)(AD)^T C(AD) \det \boldsymbol{J} d\xi d\eta \,, \quad (27)$$

where $w(d)$ is the degradation function and C is the elastic coefficient matrix.

The stiffness matrix for the phase field is expressed as:

$$K^{dd} = -\frac{\partial R_l^d}{\partial d^e} = \int_{\Omega^e} H(\psi^+) w''(d)(N_d)^T N_d \det \boldsymbol{J} d\xi d\eta + \int_{\Omega^e} \frac{G_c}{l_0}[(N_d)^T N_d + l_0^2 (B_d)^T (B_d)] \det \boldsymbol{J} d\xi d\eta, \quad (28)$$

where N_d is the unit shape function matrix corresponding to the phase field, $H(\psi^+)$ is a historical variable and G_c is the critical energy release rate.

The formulas for calculating the Right-Hand Side (RHS) are as follows.

$$\boldsymbol{R}^u = -\left[\int_{\Omega^e} w(d)(AD)^T C(AD) \det \boldsymbol{J} d\xi d\eta\right] \boldsymbol{U} + \int_{\Omega^e} \boldsymbol{N}^T \cdot \boldsymbol{f} \det \boldsymbol{J} d\xi d\eta + \int_{\partial\Omega_t} \boldsymbol{N}^T \cdot \boldsymbol{t} dS, \quad (29)$$

$$\boldsymbol{R}^d = -\left\{\int_{\Omega^e} \frac{G_c}{l_0}[\boldsymbol{N}_d^T \boldsymbol{N}_d + l_0^2 (B_d)] \det \boldsymbol{J} d\xi d\eta\right\} d^e - \int_{\Omega^e} w'(d) \psi^+(\varepsilon) \boldsymbol{N}_d^T \det \boldsymbol{J} d\xi d\eta, \quad (30)$$

where $\boldsymbol{U}$ is the node vector of the displacement field at the element node, $\boldsymbol{N}$ is the element shape function matrix corresponding to the displacement field and $\boldsymbol{f}$ represents the mass density of the material.

2.2. Model

We referenced the two-dimensional model of the Haversian canal established in the anterior anatomical region in [15] to construct our model in ABAQUS. The model captures the intricacies of the bone unit, which includes a 150 μm diameter, elliptical lacunae measuring 8.56 μm along the long axis and 3.82 μm along the short axis, and adhesive lines that are 1 μm thick. A series of five models is developed to investigate the biomechanical implications of lacunae and perilacunar zones within the bone matrix, as shown in Fig. 2. Model 1 serves as a control, devoid of lacunae, while Model 2 features a lacuna in close proximity to the Haversian canal. Model 3 is analogous but positions the lacuna near the adhesive line. Models 4 and 5 extend this investigation by incorporating perilacunar zones, which are offset by 5 μm from the positions in Models 2 and 3, respectively.

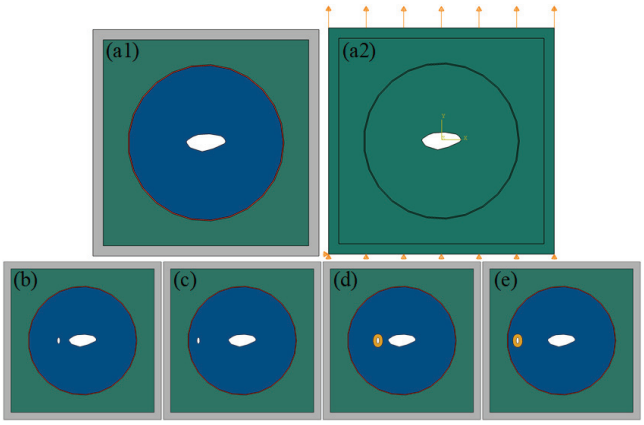

Fig. 2. Single bone unit models: (a) Model 1, (b) Model 2, (c) Model 3, (d) Model 4, (e) Model 5

In this work, the material properties, including elastic modulus, critical energy release rate and Poisson's ratio, were determined based on previous research studies and experimental measurements [9], [20], as shown in Table 1. However, it is important to note that the micro-mechanical behavior of certain materials, such as the bone interstitial and perilacunar zone, is difficult to precisely quantify due to individual variations, age-related changes and anatomical factors.

Table 1. Material properties for the single bone unit model

Material	Elastic modulus [GPa]	Poisson's ratio	Critical energy release rate [N/mm]
Homogenized	18.15	0.25	0.57
Interstitial	19.70	0.25	0.52
Cement line	12.45	0.30	0.1629
Osteon	16.60	0.25	0.62
Perilacunar	15.00	0.25	0.65

The construction of the Haversian canal model is confirmed by SEM imagery, capturing the stochastic nature of their distribution, as depicted in Fig. 3.

Microcracks predominantly originate and disseminate from the Haversian canal, a process that is exacerbated by lacunae, which serve as focal points for stress concentration. To evaluate their influence on the mechanical properties of cortical bone, a series of models have been crafted.

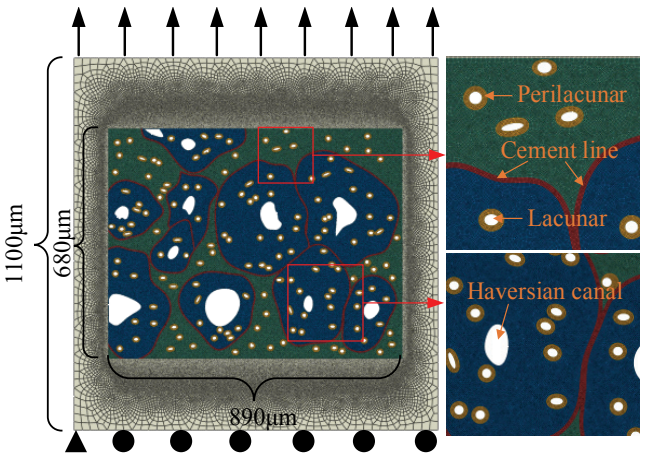

Fig. 3. Multi-osteon crack propagation finite element model

The models incorporate a bone cement line with a thickness of 5 μm, and approximately 150 lacunae are dispersed in a manner consistent with the distribution patterns outlined in a seminal study [15]. This distribution is further confirmed by the empirical relationship established by Vashishth et al. [32], [33]. The models are as follows: Model 6, devoid of lacunae; Model 7, featuring a random distribution of lacunae; and Model 8, which is analogous to Model 7 but includes an additional perilacunar zone, offset by 5 μm. These models are integrated into a multi-bone unit configuration, measuring 890 μm × 680 μm, and are encapsulated within a larger 1100 μm × 1100 μm square plate, as illustrated in Fig. 4. This comprehensive approach allows for a detailed investigation into the structural and mechanical implications of the Haversian canal system and its associated microarchitecture. In the finite element analysis process, tensile loading is applied to the model. Tensile loading induces stress concentration near the crack tip, which is crucial for driving crack propagation and facilitating insightful analysis.

3. Results

To accurately model the system, an optimal mesh size of 0.25 μm and length dimension parameter of 0.5 μm were determined. In Figure 5, grid convergence assessment with varying mesh sizes is illustrated. Microcrack damage and crack length variation stabilized at 0.2 μm, indicating refinement sufficiency. All models utilized meshes ranging from 510 000 to 530 000, ensuring comprehensive analysis.

Microcracks typically initiate from the Haversian canal, as shown in Fig. 5, which is consistent with the simulation results. The process of microcrack propagation is illustrated in Fig. 6. In Model 1, the crack length at each tensile displacement node is smaller than that of the other models, as depicted in Fig. 6 (a). In contrast, the crack length in Model 2 is significantly larger than that of the other models. By withstanding a tensile displacement of 7.4 μm, microcracks have already propagated through the bone cavity and continued to expand, as shown in Fig. 6 (b2).

In Model 4, the crack, influenced by perilacunar zones, has not yet penetrated lacunae and its length is smaller than that of Model 2 under the same tensile displacement, as illustrated in Fig. 6 (d2). Additionally, it can be observed that the peri-implant cavity delays the expansion of microcracks and reduces their length by comparing Model 3 with Model 5 (Fig. 6 (c3) and (e3)).

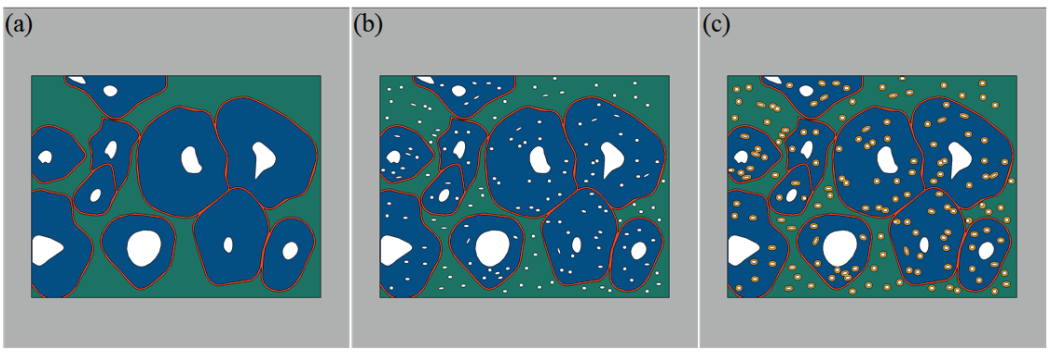

Fig. 4. Multi-osteon models: (a) Model 6 (no lacunae), (b) Model 7 (with lacunae), and (c) Model 8 (with lacunae and perilacunar zones)

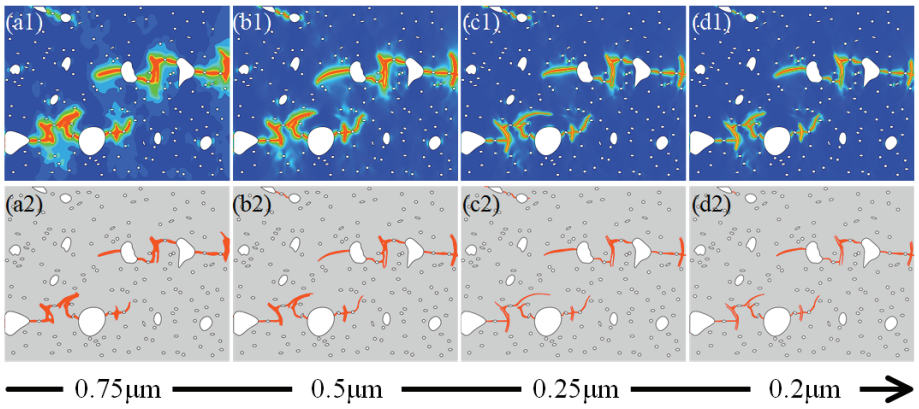

Fig. 5. Mesh size parameter evaluation: (a) 0.75 μm, (b) 0.5 μm, (c) 0.25 μm, (d) 0.2 μm

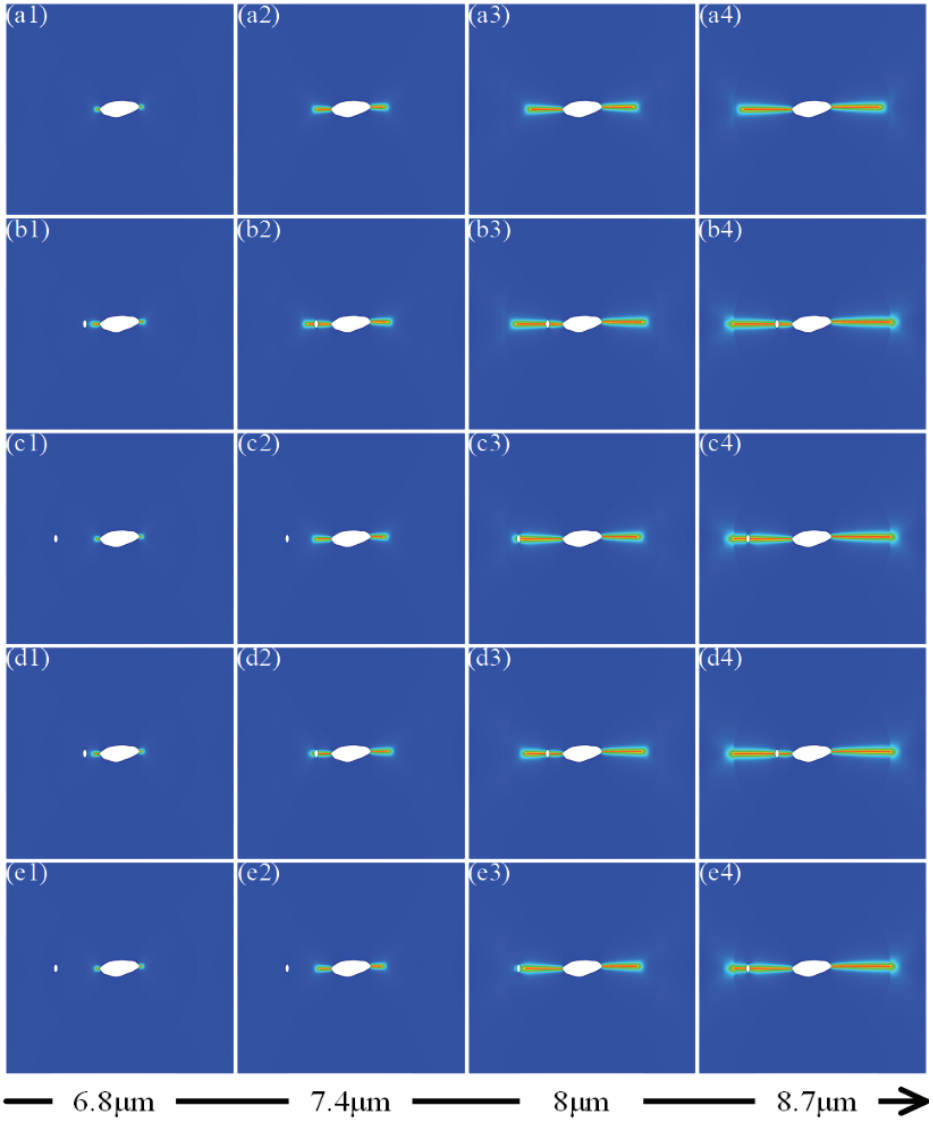

Fig. 6. Crack propagation in single bone unit models: (a) Model 1, (b) Model 2, (c) Model 3, (d) Model 4, (e) Model 5

In Figure 7, the variation in the number of damaged elements with tensile displacement in five single bone unit models is illustrated. In contrast to lacuna-absent Model 1, the presence of a lacuna amplifies damage, influenced by the spatial relation to the Haversian canal. Model 2, illustrated in Fig. 7a, displays notably higher damage, with concentrated initiation points near the Haversian canal. The adjacency of lacunae acts as an

amplifier, increasing the susceptibility of microcracks to propagate from the Haversian canal compared to other models.

In Figure 7b, from 6.8 μm to 7.9 μm, Model 3 mimics Model 1's crack propagation. Yet, between 7.9 μm and 8.7 μm, Model 3 exhibits higher damage. Initially, microcracks parallel Models 1 and 3, but encountering lacunae introduces new damage initiation sites, facilitating increased propagation in Model 3. Perilacunar zones, in Fig. 7c and d, significantly reduce damage, aligning with their proposed protective role, hindering and delaying crack initiation and propagation by offering support and resisting growth.

In Figures 8 and 9, grayscale and phase field images are displayed respectively, illustrating damage evolution in multi-bone unit models. Microcracks predominantly

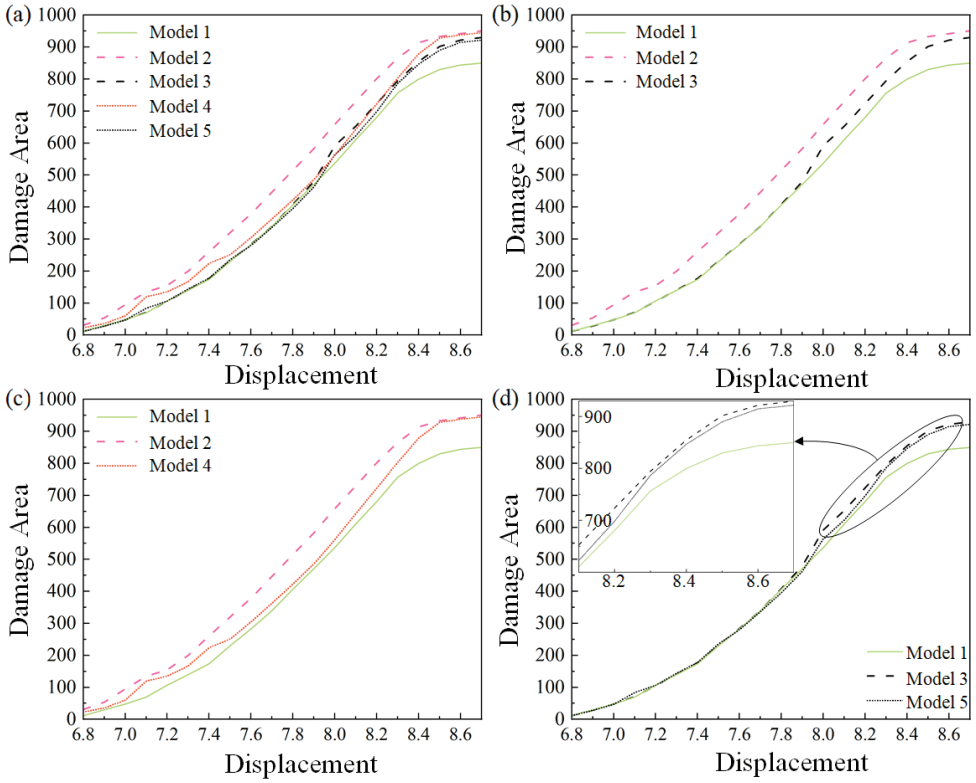

Fig. 7. Variation in the number of damaged elements with tensile displacement in five single bone unit models

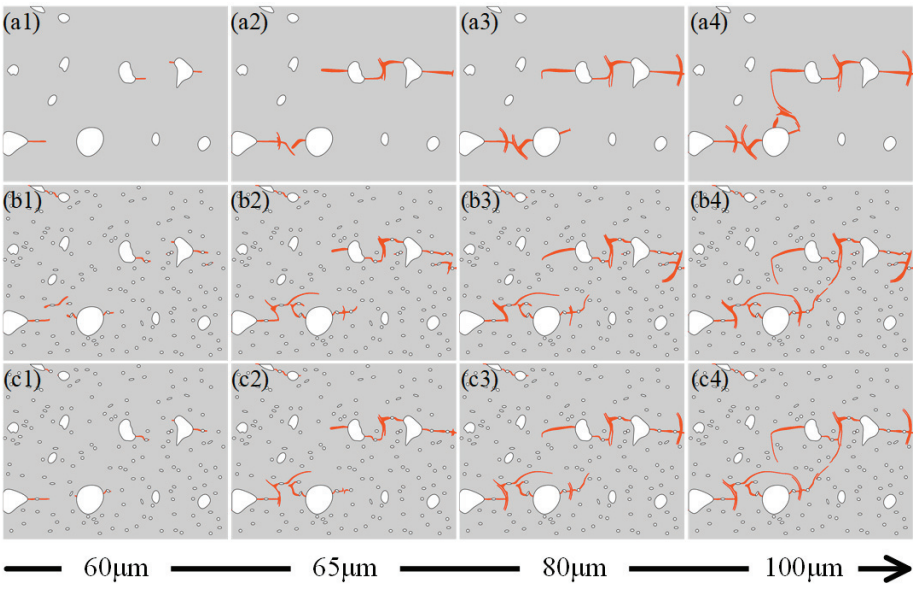

Fig. 8. Grayscale images of damage evolution in multi-bone unit models: (a) Model 6 (no lacunae), (b) Model 7 (with lacunae), (c) Model 8 (with lacunae and perilacunar zones)

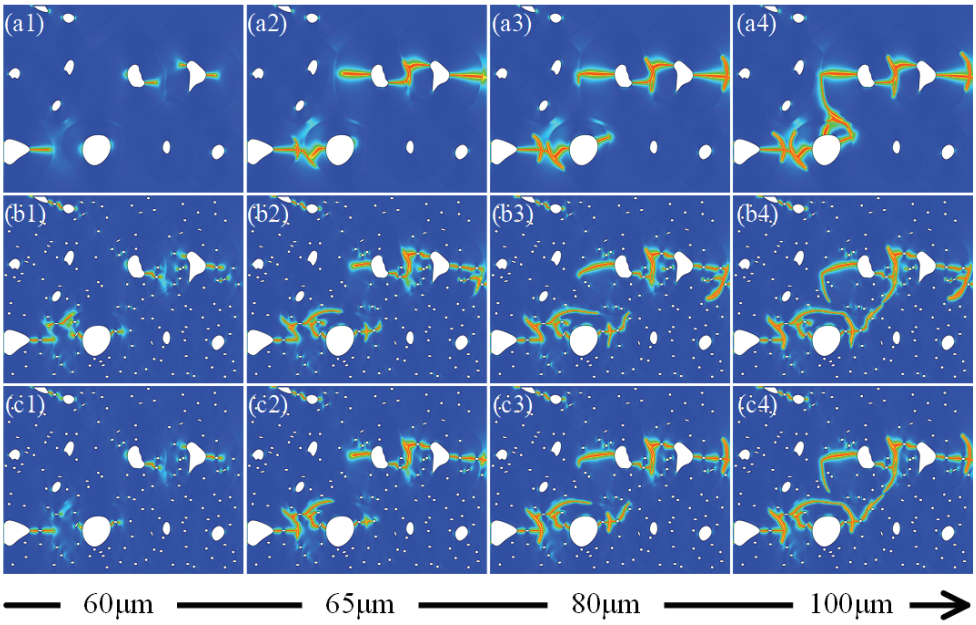

Fig. 9. Phase field diagram of damage evolution in multi-bone unit models: (a) Model 6 (no lacunae), (b) Model 7 (with lacunae), (c) Model 8 (with lacunae and perilacunar zones)

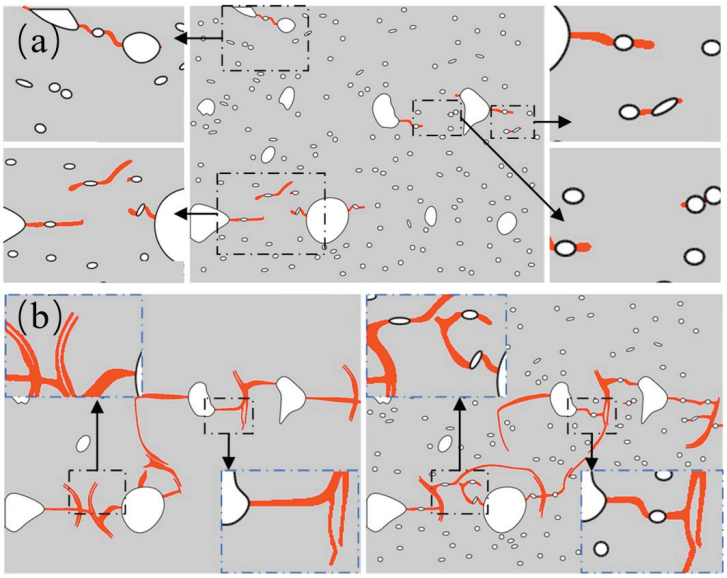

Fig. 10. Schematic of crack propagation in multi-bone unit models: (a) originating from bone lacunae, (b) local propagation path

originate from the Haversian canal, with lacunae altering crack propagation direction. When microcracks extend from the Haversian canal to interstitial bone, they act as external cracks. Extending towards other bone units, these cracks deviate near cement lines, ensuring bone unit integrity – an effect termed toughening by bone cement lines. These results align with experiments by Josephson [15] and Chan et al. [5].

The presence of lacunae introduces novel sites for damage initiation, significantly amplifying the overall extent of damage when compared to models devoid of these structures (Fig. 10a). Microcracks are nucleated in regions of heightened stress concentration proximal to lacunae and progressively propagate over successive loading cycles, thereby escalating the propensity for fracture. Additionally, lacunae serve as "trapping points" that alter the trajectory of microcracks (Fig. 10b). They induce minor deviations in the path of adjacent microcracks, effectively directing their progression along specific routes.

Moreover, the perilacunar zone exerts a dual effect on microcrack propagation, manifesting in two distinct

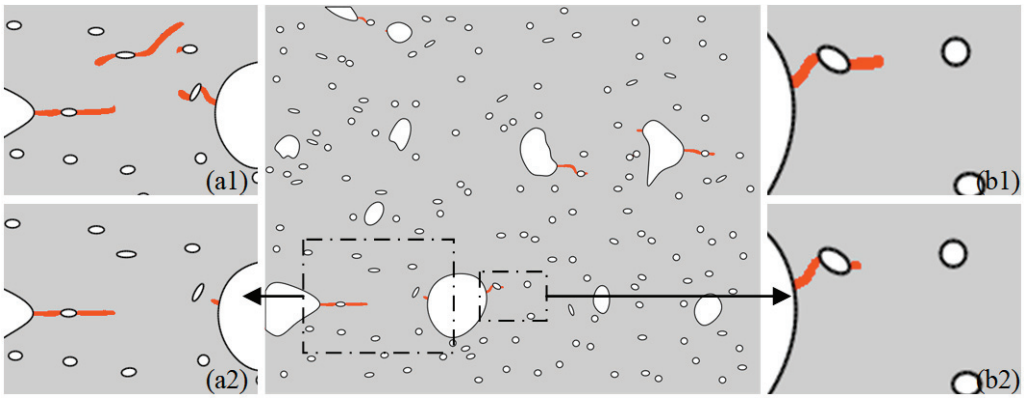

Fig. 11. Inhibitory effect of perilacunar zone (tensile displacement 60 μm): (a1) without perilacunar zone, (a2) with perilacunar zone, (b1) without perilacunar zone, (b2) with perilacunar zone

manners: firstly, it acts as a deterrent to the initiation of microcracks in the vicinity of lacunae, as illustrated in Fig. 11a; secondly, it impedes the propagation of microcracks upon their penetration into the perilacunar zone, thereby preventing further advancement. The capturing effect of lacunae on microcracks precedes the inhibitory influence of the perilacunar zone. The elevated stress concentration surrounding lacunae channels microcracks towards them, establishing pathways before encountering the perilacunar zone where the inhibitory effects become operational (refer to Fig. 11b).

4. Discussion

In this study, we aimed to delve into the microstructural characteristics of cortical bone, particularly lacunae and the surrounding perilacunar zones, and their biomechanical implications on microdamage accumulation. To comprehensively evaluate the impact of these microstructural elements on the biomechanical properties of cortical bone, we conducted a series of computational simulations using the phase field finite element method.

Different methods have been employed to capture the damage mechanisms at the microscale of cortical bone. Barros utilized the Mesh Fragmentation Technique (MFT) to highlight the role of the cement line in crack propagation [1]. Gustafsson employed the Extended Finite Element Method (XFEM) to study crack trajectories, emphasizing the importance of the cement line interface [11]. In contrast, Josephson utilized phase field finite element models to investigate the impact of osteocyte activity on microcracking, revealing the potential of perilacunar zones to delay or prevent crack propagation [15]. Like Josephson, we utilized the phase field method to offer a comprehensive understanding of bone microstructure mechanics by integrating cellular processes with mechanical behavior, thereby providing valuable insights for future research in bone biomechanics and tissue engineering. However, our damage mathematical model and the finite element model differ.

The results presented in Figs. 9 and 10a are consistent with experimental studies on microcrack initiation and propagation in bone units by Reilly [26] and Voide [31]. The results indicate that microcracks primarily originate from the Haversian canal, while the lacunae alter the direction of crack propagation, which is like the simulated results in this study (Fig. 10b). Voide's results also indicate that microcracks usually do not originate from lacunae. However, Reilly reached the opposite conclusion, finding a high frequency of microcrack initiation from lacunae. Although in this section, lacunae are indeed the starting point of damage, compared to Model 2, the damage starting from lacunae in Model 3 is significantly reduced or delayed, which may indicate that the perilacunar zones affect the reduction of microdamage starting from lacunae in Voide's experimental research. Additionally, differences in loading conditions may further explain the differences in lacunar damage initiation, as Voide et al. studied axial compression while Reilly studied tensile microdamage.

Regarding the role of perilacunar zones in cortical bone microdamage behavior, different studies have proposed conflicting conclusions. Reilly et al. [26] believe that perilacunar zones act as stress concentrators, increasing microdamage, while Vashishth et al. [30], [31] found that microcracks are more common in areas lacking osteocytes, meaning the presence of perilacunar zones reduces microcracks. The simulation results in this section suggest that these two views are not contradictory. The results indicate that while perilacunar zones do lead to stress concentration, the ability of

osteocytes to remodel the surrounding bone matrix slows down or prevents microcrack formation. Although this may not prevent substantial linear microcracks and subsequent fractures in cortical bone under significant loads, the presence of perilacunar zones does delay the process of microcrack propagation, providing time for local remodeling by osteocytes and helping to prevent the accumulation of microcracks.

Another critical aspect addressed in our study is the influence of the perilacunar zone on microcrack propagation. We found that this region, characterized by sub-micrometer modulus gradation [27], plays a protective role by delaying the propagation of microcracks, thereby facilitating localized remodeling and preventing the accumulation of microdamage. This aligns with the observations of Voide et al. [31] regarding the importance of murine cortical bone microstructure in microcrack dynamics.

Our research builds upon and extends previous studies by integrating the phase field method, which has been instrumental in analyzing fracture resistance and the impact of advanced glycation end products (AGEs) on cortical bone fracture, as demonstrated by Da et al. [7] and Maghami et al. [24]. This comprehensive approach provides valuable insights into the biomechanical response of cortical bone to stress, highlighting the significance of microarchitectural features in the development of targeted therapeutic strategies and biomimetic materials.

Summaring, our study contributes to the advancement of knowledge on how lacunae and perilacunar zones in cortical bone microarchitecture influence biomechanical properties. By considering these microarchitectural features, we can better understand and address bone-related disorders, such as osteoporosis and skeletal fragility syndromes, ultimately aiming to improve clinical outcomes for affected patients.

Although this paper has simulated and analyzed the relationship between bone unit microstructure and microcrack propagation, due to the complex nature of biological materials, the complex environmental factors in the body, and the limitations of the study time, there are some limitations to this paper. First, regarding the finite element model of bone units, only one bone unit model was used for analysis, which cannot represent the distribution morphology of bone units in different parts and age groups of the femur. However, there is currently a lack of statistical analysis and a unified model of bone unit distribution. In addition, the characteristics of microcracks caused by lacunae, both in the early and late stages, have been verified through SEM images and related experiments, but further experimental studies are needed on the middle stage of microcrack propagation. In the analysis of the relationship between perilacunar zones and microcrack propagation, it is assumed that all remodeling processes are in the same stage, but remodeling may be in different stages. Therefore, further research is needed on the different stages of remodeling. Additionally, there is a lack of comparison between different methods for capturing microscale damage mechanisms in cortical bone.

Future work may include statistical analysis of the distribution of bone units in different parts and age groups, establishing a more universal model, and verifying and comparing the effects of several different methods for capturing microscale damage mechanisms in cortical bone.

5. Conclusions

This research utilized fracture phase field models to scrutinize the accumulation of microdamage in cortical bone subjected to tensile loading, focusing on the roles of lacunae and perilacunar zones. The study's pivotal discoveries are as follows:

1. Lacunae within compact bone significantly elevate the propensity for microcrack initiation, acting as focal points that expedite the propagation of microcracks;
2. The lacunae can alter the extent, rate, and mode of microcrack propagation. The presence of lacunae increases the risk of microcrack initiation. They can serve as preferential sites for microcrack initiation, thereby accelerating crack propagation;
3. Lacunae can modify the propagation path of microcracks, acting as "trapping points" for microcracks, causing nearby microcracks to deflect. Prior to the protective effects of perilacunar zones, lacunae exert a trapping effect on microcracks, steering their propagation towards these regions;
4. The propagation of microcracks is relatively unresponsive to variations in the elastic modulus. However, an increase in the critical energy release rate effectively decelerates microcrack growth, resulting in a reduction of damaged grid cells and the overall area affected by cracks.

Summarizing, this study constructed fracture propagation models incorporating single and multiple bone units, simulated microdamage accumulation in bone units under tensile loading using fracture phase-field computational methods and investigated the influence of lacunae and perilacunar zones formed during local remodeling by bone cells on cortical bone fracture

behavior. These insights contribute to a more nuanced understanding of bone fracture mechanics, which is instrumental in devising effective preventive strategies and improving fracture treatment protocols. The implications of these findings are far-reaching, potentially informing the development of novel therapeutic approaches and biomimetic materials designed to enhance bone integrity and resilience.

Competing interests

The authors declares that they have no competing interests.

Acknowledgements

This work is supported by the National Natural Science Foundation of China (No. 32271432, 12302420, 52305513).

References

[1] BARROS M.A.M.D., MANZOLI O.L., BITENCOURT L.A.G., *Computational modeling of cracking in cortical bone microstructure using the mesh fragmentation technique*, Arch. Appl. Mech., 2024.

[2] BOURDIN B., FRANCFORT G.A., MARIGO J.J., *Numerical experiments in revisited brittle fracture*, J. Mech. Phys. Solids, 2000, 48, 797–782.

[3] BOUAZIZ O., PARDOEN T., *Phase field modeling of fracture: A powerful tool to understand material failure*, J. Mech. Phys. Solids, 2019, 123, 104–144.

[4] CARLSSON J., BRAESCH-ANDERSEN A., FERGUSON S.J., ISAKSSON P., *Fracture in porous bone analyses with a numerical phase-field dynamical model*, J. Mech. Behav. Biomed. Mater., 2023, 139, 105659.

[5] CHAN K.S., CHAN C.K., NICOLELLA D.P., *Relating crack-tip deformation to mineralization and fracture resistance in human femur cortical bone*, Bone, 2009, 45, 427–434.

[6] DOMINGUEZ V.M., AGNEW A.M., *Microdamage as a bone quality component: practical guidelines for the two-dimensional analysis of linear microcracks in human cortical bone*, JBMR Plus., 2019, 3 (6), 1–15.

[7] DA D., QIAN X., *Fracture resistance design through biomimicry and topology optimization*, Extreme Mech. Lett., 2020, 40, 100890.

[8] DONALDSON F., RUFFONI D., SCHNEIDER P., LEVCHUK A., ZWAHLEN A., *Modeling microdamage behavior of cortical bone*, Biomech. Model. Mechanobiol., 2014, 13 (6), 1227–1242.

[9] GINER E., BELDA R., ARANGO C., VERCHER-MARTINEZ A., *Calculation of the critical energy release rate Gc of the cement line in cortical bone combining experimental tests and finite element models*, Eng. Fract. Mech., 2017, 184, 168–182.

[10] GANESH T., LAUGHREY L.E., NIROOBAKHSH M., NURIA L.C., *Multiscale finite element modeling of mechanical strains and fluid flow in osteocyte lacunocanalicular system*, Bone, 2020, 137, 115328.

[11] GUSTAFSSON A., KHAYYERI H., WALLIN M., ISAKSSON H., *An interface damage model that captures crack propagation at the microscale in cortical bone using XFEM*, J. Mech. Behav. Biomed. Mater., 2019, 90, 556–565.

[12] GUSTAFSSON A., WALLIN M., KHAYYERI H., ISAKSSON H., *Crack propagation in cortical bone is affected by the characteristics of the cement line: a parameter study using an XFEM interface damage model*, Biomech. Model. Mechan., 2019, 18, 1247–1261.

[13] HOENIG T., ACKERMAN K.E., BECK B.R., BOUXSEIN M.L., BURR D.B., *Bone stress injuries*, Nat. Rev. Dis. Primers, 2022, 26.

[14] IEZZI G., MANGANO C., BARONE A. et al., *Jawbone remodeling: a conceptual study based on synchrotron high-resolution tomography*, Sci. Rep., 2020, 3777.

[15] JOSEPHSON T.O., MOORE J.P., MAGHAMI E., FREEMAN T.A. NAJAFI A.R., *Computational study of the mechanical influence of lacunae and perilacunar zones in cortical bone microcracking*, J. Mech. Behav. Biomed. Mater., 2022, 126, 105029.

[16] JANKOWSKI K., PAWLIKOWSKI M., BARCZ K., *Some aspects related to the indentation-based viscoelastic modelling of trabecular bone tissue*, Acta Bioeng. Biomech., 2022, 24 (3), 169–177.

[17] JI C.H., ZHANG L., WANG Y., LIN B., BAI X.L., YUN S.Y., HE B.N., *The influence of different shaped osteocyte lacunae on microcrack initiation and propagation*, Clin. Biomech., 2023, 108, 106072.

[18] KOLA S.K., BEGONIA M.T., TIEDE-LEWIS L.M., LAUGHREY L.E., DALLAS S.L., JOHNSON M.L., GANESH T., *Osteocyte lacunar strain determination using multiscale finite element analysis*, Bone Rep., 2020, 100277.

[19] KOPERNIK M., DYRDA K., KURYTKA P., MAJOR R., *Discrete phase model of blood flow in a roughness microchannel simulating the formation of pseudointima*, Acta Bioeng. Biomech., 2022, 24 (1), 131–144.

[20] LI S., ABDEL-WAHAB A., DEMIRCI E., SILBERSCHMIDT V.V., *Fracture process in cortical bone: X-FEM analysis of microstructure models*, Int. J. Fract., 2013, 184, 43–55.

[21] LI J., GONG H., *Fatigue behavior of cortical bone: a review*, Acta Mech. Sin., 2021, 37, 516–526.

[22] MOLNAR G., GRAVOUIL A., *2D and 3D Abaqus implementation of a robust staggered phase-field solution for modeling brittle fracture*, J. Finite Elem. Anal. Des., 2017, 130, 27–38.

[23] MIEHE C., HOFACKER M., WELSCHINGER F., *A phase field model for rate-independent crack propagation: Robust algorithmic implementation based on operator splits*, J. Comp. Methods Appl. Mech. Eng., 2010, 199, 2765–2778.

[24] MAGHAMI E., JOSEPHEON T.O., MOORE J.P., RWZAEE T., FREEMAN T.A., KARIM L., NAJAFI A.R., *Fracture behavior of human cortical bone: Role of advanced glycation end-products and microstructural features*, J. Biomech., 2021, 125, 110600.

[25] MORIISHI T., KOMORI T., *Osteocytes: Their lacunocanalicular structure and mechanoresponses*, Int. J. Mol. Sci., 2022, 23, 4373.

[26] REILLY G.C., *Observations of microdamage around osteocyte lacunae in bone*, J. Biomech., 2000, 1131–1134.

[27] RUX C.J., VAHIDI G., DARABI A., COX L.M., HEVERAN C.M., *Perilacunar bone tissue exhibits sub-micrometer modulus gradation which depends on the recency of osteocyte bone formation in both young adult and early-old-age female C57Bl/6 mice*, Bone, 2022, 157, 116327.

[28] WITTIG N.K., LAUGESEN M., BIRKBAK M.E., BACH-GANSMO F.L., PACUREANU A., BRUNS S., WENDELBOE M.H., BRÜEL A., SØRENSEN H.O., THOMSEN J.S., BIRKEDAL H., *Canalicular*

Junctions in the Osteocyte Lacuno-Canalicular Network of Cortical Bone, ACS Nano, 2019, 13 (6), 6421–6430.

[29] SALHOTRA A., SHAH H.N., LEVI B., LONGAKE M.T., *Mechanisms of bone development and repair*, Nat. Rev. Mol. Cell Biol., 2020, 696–711.

[30] SANG W., URAL A., *Quantifying how altered lacunar morphology and perilacunar tissue properties influence local mechanical environment of osteocyte lacunae using finite element modeling*, J. Mech. Behav. Biomed. Mater., 2022, 135, 105433.

[31] VOIDE R., SCHNEIDER P., STAUBER M., HARRY G.H., STAMPANONOI M., *The importance of murine cortical bone microstructure for microcrack initiation and propagation*, Bone, 2011, 1186–1193.

[32] VASHISHTH D., TANNER K.E., BONFIELD W., *Contribution, development and morphology of microcracking in cortical bone during crack propagation*, J. Biomech., 2000, 33, 1169–1174.

[33] VASHISHTH D., VERBORGT O., DIVINE G., FYHRIE D.P., *Decline in osteocyte lacunar density in human cortical bone is associated with accumulation of microcracks with age*, Bone, 2000, 375–380.

[34] VERBRUGGEN S.W., VAUGHAN T.J., MCNAMARA L.M., *Strain amplification in bone mechanobiology: a computational investigation of the in vivo mechanics of osteocytes*, J. R. Soc. Interface, 2012, 75, 2735–2744.

[35] WENTZELL S., NESBITT R.S., MACLONE J., KOTHA S., *Measurement of lacunar bone strains and crack formation during tensile loading by digital volume correlation of second harmonic generation images*, J. Mech. Behav. Biomed. Mater., 2016, 148–156.

[36] WANG L., YOU X., ZHANG L., ZHANG C.Q., *Mechanical regulation of bone remodeling*, Bone Res., 2022, 16.

[37] YU B., PACUREANU A., OLIVIER C., CLOETENS P., PEYRIN F., *Assessment of the human bone lacuno-canalicular network at the nanoscale and impact of spatial resolution*, Sci. Rep., 2020, 4567.

[38] YU X., WANG R., DONG C., JI J.Y., ZHEN X.X., *3D implementation of push-out test in ABAQUS using the phase-field method*, J. Mech. Sci. Technol., 2023, 37, 1731–1745.

[39] ZHANG X., WANG J., *Phase field modeling of crack initiation and propagation in composite materials*, Compos. Part B: Eng., 2021, 206, 108691.